Cerebral Cortex December 2009;19:2891–2901
doi:10.1093/cercor/bhp068
Advance Access publication April 20, 2009

Hypoxic Injury during Neonatal Development in Murine Brain: Correlation between In Vivo DTI Findings and Behavioral Assessment

Halima Chahboune[1,2,3], Laura R. Ment[4], William B. Stewart[5], Douglas L. Rothman[1,2,3,6], Flora M. Vaccarino[7,8], Fahmeed Hyder[1,2,3,6] and Michael L. Schwartz[7]

[1]Department of Diagnostic Radiology, [2]Center for Quantitative Neuroscience with Magnetic Resonance (QNMR), [3]Magnetic Resonance Research Center (MRRC), [4]Departments of Pediatrics, [5]Surgery, [6]Biomedical Engineering, [7]Neurobiology and [8]Child Study Center, Yale University, New Haven, CT 06510, USA

Preterm birth results in significant neurodevelopmental disability. A neonatal rodent model of chronic sublethal hypoxia (CSH), which mimics effects of preterm birth, was used to characterize neurodevelopmental consequences of prolonged exposure to hypoxia using tissue anisotropy measurements from diffusion tensor imaging. Corpus callosum, cingulum, and fimbria of the hippocampus revealed subtle, yet significant, hypoxia-induced modifications during maturation (P15–P51). Anisotropy differences between control and CSH mice were greatest at older ages (>P40) in these regions. Neither somatosensory cortex nor caudate putamen revealed significant differences between control and CSH mice at any age. We assessed control and CSH mice using tests of general activity and cognition for behavioral correlates of morphological changes. Open-field task revealed greater locomotor activity in CSH mice early in maturation (P16–P18), whereas by adolescence (P40–P45) differences between control and CSH mice were insignificant. These results may be associated with lack of cortical and subcortical anisotropy differences between control and CSH mice. Spatial-delayed alternation and free-swim tasks in adulthood revealed lasting impairments for CSH mice in spatial memory and behavioral laterality. These differences may correlate with anisotropy decreases in hippocampal and callosal connectivities of CSH mice. Thus, CSH mice revealed developmental and behavioral deficits that are similar to those observed in low birth weight preterm infants.

Keywords: axon, brain development, diffusivity, hypoxia, preterm birth

Introduction

Preterm birth is a major cause of neurodevelopmental disability. Almost 1% of all live births in the United States are infants weighing less than 1000 g and the survival rate of these preterm infants is between 60% and 85% (Guyer et al. 1999; Bassan et al. 2006). Depending on the birth weight of the studied population and the year of birth, the incidence of major cognitive handicaps in this population of infants ranges from 30% to 50%. At age of 8 years, more than 50% of these children require special assistance in the classroom, about 20% are in special education, and nearly 15% have repeated at least one grade in school (Saigal and Doyle 2008).

Circulatory disturbances and oxygen deprivation are major causes of neurodevelopmental disability in preterm infants (Volpe 1990; Saigal 2000). Prematurely born infants have prominent reductions in cerebral gray and white matter, as well as volume reduction in subcortical gray matter regions when compared with full term infants (Peterson et al. 2000; Inder et al. 2005). Correlations of volumetric changes in brain structure with adverse neurodevelopmental outcome have been reported for a variety of measures including the Wechsler IQ, visuomotor functioning, and behavioral problems at school age and adolescence (Reiss et al. 2004; Gimenez et al. 2006; Nosarti et al. 2008). Moreover, the degree of volume loss in the amygdala, the parietal, temporal, and sensorimotor cortices, as well as white matter regions including the corpus callosum, are all considered to be positive predictors of poor cognitive outcomes (Peterson et al. 2000). Postnatal hypoxia resulting from lung immaturity and respiratory disturbances in these infants has been hypothesized to be an important pathophysiological mechanism underlying these devastating neurological complications.

Consistent with the neuropathologic sequelae in preterm infants, the brains of rats and mice exposed to chronic sublethal hypoxia (CSH) within the first weeks of postnatal life are characterized by decreased cortical volume and paucity of subcortical white matter (Laroia et al. 1996; Turner et al. 2003; Schwartz et al. 2004). Prolonged chronic hypoxia is a common problem of very low birth weight preterm infants, and several investigators have recently employed magnetic resonance imaging (MRI) to demonstrate that this environmental perturbation significantly alters cerebral structure in preterm birth (Boardman et al. 2007; Thompson et al. 2007). The newborn mouse provides a good model to study the impact of environmental factors on brain development in preterm birth. The interval during which our CSH rodent model is employed is generally considered to represent the third trimester of human gestation, the time during which many very low birth weight preterm infants experience the developmental sequence of respiratory distress syndrome, bronchopulmonary dysplasia, and ultimately chronic lung disease (Haddad and Jiang 1993; Volpe 1997).

Many of the structural changes that occur during the initial postnatal period in rodents are consistent with those seen during the late prenatal period in human brain development. For example, similar to the end of the second trimester in preterm human infants, the newborn rodent has completed cortical neuron generation, while axonal and dendritic growth, branching and gliogenesis are ongoing (Rothblat and Hayes 1982; Olavarria and Van Sluyters 1985; Ferrer et al. 1992) and synaptogenesis is beginning (Dobbing 1972). Thus, exposure of mice to hypoxia from postnatal days 3 to 11 (P3–P11) includes many of the neurodevelopmental events that may be affected by hypoxia in preterm human infants. This model was developed by G.G. Haddad and has been used by numerous investigators to investigate brain development in the prematurely born (Zhou et al. 2008). In the present study we used in vivo diffusion tensor imaging (DTI) of CSH and control mice in conjunction with cognitive tests to assess the structural and

behavioral consequences of prolonged exposure to hypoxia during brain development.

DTI with high field MRI is emerging as a sensitive tool for imaging anatomical connectivity (Mori and van Zijl 1995; Nakada and Matsuzawa 1995; Xue et al. 1999), microstructural morphology in the brain (Mori et al. 2001; Zhang et al. 2002, 2003), and for characterizing developmental disorders such as cerebral palsy (Drobyshevsky et al. 2007). In addition, DTI is useful for assessing diffuse brain injury (Sizonenko et al. 2007) and characterizing neurodegenerative diseases such as Wallerian degeneration (Mazumdar et al. 2003), Alzheimer's disease (Song et al. 2004; Sun et al. 2005), multiple sclerosis (Budde et al. 2007), and Parkinson's disease (Boska et al. 2007).

Briefly, we found that some cortical and subcortical regions (e.g., somatosensory cortex, caudate putamen) were unaffected by hypoxia, whereas some white matter areas (e.g., corpus callosum, cingulum, fimbria of the hippocampus) revealed hypoxia-induced modifications during development. Test results of open-field activity, spatial-delayed alternation, and free-swim behaviors were found to correlate with the neuroanatomical findings revealed using DTI. These results suggest that prolonged exposure to hypoxia in neonatal mice results in anatomical and behavioral deficits in CSH mice that are similar to those observed in low birth weight preterm infants.

Materials and Methods

CSH Model

C57B/L6 litters (P15–P51), cofostered by CD1 dams, were reared under hypoxia (CSH; ambient oxygen = 9.5 ± 1.0%) or normal conditions (control; ambient oxygen = 22 ± 1.0%) from P3 to 11. Hypoxic exposure was conducted in a Plexiglas chamber (BioSpherix, Ltd, Lacona, NY) equipped with a small fan to provide forced circulation and almost instantaneous homogenization of gases within the chamber. The oxygen content of the chamber was adjusted by a nitrogen/compressed air gas delivery system that mixes the nitrogen with room air using a compact oxygen controller (BioSpherix, Ltd, Pro:OX). Temperature, lighting, and humidity were maintained at standard vivarium levels and the chamber was opened for 5–10 min biweekly for routine care. In initial studies, we observed that C57B/L6 dams were inconsistent in attending to their litters within the hypoxia chamber. Thus, we cofostered C57B/L6 litters with CD1 dams for both control and CSH litters of mice. CD1 fostering of C57B/L6 litters was performed by pairing a timed pregnant CD1 dam and a C57B/L6 dam in the same cage prior to delivery. One to 2 days after birth, CD1 litters were culled to 3 pups. A maximum pup census of 13 mice was maintained in the group cages prior to weaning.

Animal Preparation for DTI

For in vivo DTI studies, 5 groups of male C57B/L6 mice ($n = 6$ in each group) aged at P15, P17, P38, P45, and P51 were studied. During DTI examination, subjects were maintained under urethane anesthesia using abdominal intraperitoneal lines. Usually a single dose (1 g/kg) provides sufficient anesthetic depth for the entire DTI scan (i.e., no longer than 1 h). However, in some cases, supplemental doses (0.1g/kg/h) were required to maintain an appropriate anesthetic level. Following induction of anesthesia, the subject was placed prone inside a cradle designed to minimize movement. A circular ^{1}H surface radio frequency coil (15 mm diameter) was then placed above the head. During DTI scanning the subject was kept warm by a hot water blanket and the core temperature was maintained within 0.5 °C by controlling the heating elements of the blanket. Whenever possible, blood samples were removed from a femoral arterial catheter at the end of the experiment to verify physiology (pH, pO_2, pCO_2).

DTI Parameters

All DTI experiments were performed using a 15-cm horizontal-bore 9.4T spectrometer (Bruker, Billerica, MA). Image orientation was coronal and contiguous slices were obtained to cover the entire brain, spanning from the olfactory bulb to the cerebellum. The magnetic field homogeneity was optimized to less than 18 Hz for the entire brain. The DTI experiment was performed using a Stejskal and Tanner spin-echo diffusion-weighted sequence (Chahboune et al. 2007): image matrix = 128 × 128 pixels; field of view = 20 × 20 mm; in-plane resolution = 156 × 156 μm; slice thickness = 500 μm; $\delta = 5$ ms; $\Delta = 8$ ms; repetition time = 1000 ms; echo time = 18 ms. Images were obtained with diffusion gradients applied in at least sixteen orientations with 2 diffusion sensitizing factors (0 and 1000 s/mm^2). DTI scans were repeated for purposes of signal averaging and/or reproducibility only if the physiological conditions allowed prolonged acquisitions.

DTI Data Analysis

The images obtained under the different orientation gradients were used in a series to test if significant translational movement (e.g., significant relaxing of the abdomen) occurred during the scan using a center of mass (COM) scheme (Chahboune et al. 2007) and the entire dataset was discarded if noticeable motion artifacts were detected as assessed from the COM shift by more than 25% of a pixel. All data that were not excluded due to movement artifact were used to calculate the independent elements of the diffusion tensor (Westin et al. 2002; Masutani et al. 2003).

Three eigenvalues (λ_1, λ_2, and λ_3) and their corresponding eigenvectors (e_1, e_2, and e_3) were calculated by matrix diagonalization to provide, respectively, the shape and orientation information from the diffusion tensor model (Basser et al. 1994; Jones et al. 1999; Hasan et al. 2001). On a pixel-by-pixel basis, the 2 most common DTI summary parameters, apparent diffusion coefficient (ADC) and fractional anisotropy (FA), were calculated using in-house software written in Matlab (The MathWorks, Inc., Natick, MA) as defined by the following equations

$$\mathrm{ADC} = \lambda_{\mathrm{avg}} = \frac{1}{3}(\lambda_1 + \lambda_2 + \lambda_3)$$

and

$$\mathrm{FA} = \sqrt{\frac{3\left(\lambda_1 - \lambda_{\mathrm{avg}}\right)^2 + \left(\lambda_2 - \lambda_{\mathrm{avg}}\right)^2 + \left(\lambda_3 - \lambda_{\mathrm{avg}}\right)^2}{2\left(\lambda_1^2 + \lambda_2^2 + \lambda_3^2\right)}}$$

where

$$\lambda_{\parallel} = \lambda_1$$

and

$$\lambda_{\perp} = \frac{1}{2}(\lambda_2 + \lambda_3).$$

In white matter of the central nervous system, $\lambda_{\parallel}$ and $\lambda_{\perp}$, respectively, represent water diffusivity parallel and perpendicular to myelinated axonal fibers and is often used to describe the degree of freedom for water to diffuse (Basser 1995). Because water moves more readily along the inside of the fiber rather than across it, $\lambda_{\parallel}$ tends to be several times higher than $\lambda_{\perp}$ (Song et al. 2002). The $\lambda_{\parallel}$ and $\lambda_{\perp}$ values are believed to respectively provide measures of intact fibers and lack of myelin. ADC and FA maps were used to depict water diffusivity respectively in nonspecific and directionally dependent manner.

In addition, the primary eigenvectors (e_1, e_2, and e_3) were used to calculate directionally encoded color (DEC) maps to highlight the orientation of anisotropic tissues using red (R), green (G), and blue (B) maps,

$$(\mathrm{R}, \mathrm{G}, \mathrm{B}) = \mathrm{FA}\left(|e_{1_x}|, |e_{1_y}|, |e_{1_z}|\right)$$

where e_1 is the eigenvector associated with the largest eigenvalues and each of these colors represent anisotropy in a directional manner (Pajevic and Pierpaoli 1999; Ennis and Kindlmann 2006). The RGB space, accomplished by merging of the 3 colors, can be used to represent the dominant anisotropy coordinates in the medial–lateral, dorsal–ventral, and anterior–posterior directions, respectively, in the coronal perspective for a rodent lying in the prone position inside

a horizontal-bore magnet (Basser and Pajevic 2003). However each of the 3 orthogonal anisotropy directions can also be represented independently (similar to the FA map) reflecting the dominant directional anisotropy (Pajevic and Pierpaoli 1999; Ennis and Kindlmann 2006).

To assess the impact of postnatal hypoxia on axonal development in mouse brain, ADC, FA, DEC, $\lambda_{\|}$, $\lambda_{\perp}$, R (medial–lateral anisotropy), G (dorsal–ventral anisotropy), and B (anterior–posterior anisotropy) maps were interrogated. Some regions of interest (ROIs)—implicated by different cognitive tasks (assessing locomotor activity, spatial memory, and behavioral laterality)—included the corpus callosum, cingulum, caudate putamen, field CA3 of hippocampus, fimbria of hippocampus, and cortical areas of the whisker barrel field and the forelimb. The ROIs were manually placed as guided by a standard mouse brain atlas (www.mbl.org) and without knowledge of the experimental group of the subject. All ROIs contained about 36 pixels (in 3-dimensional space) and varied slightly in shape given their locations across different brain regions (Fig. 1).

Animal Preparation for Behavioral Testing

Mice used for behavioral analysis were litter mates of mice examined using DTI scans. Male C57B/L6 mice for behavioral analysis were reared under hypoxia or normal conditions from P3 to P11 and then maintained in a normal environment until the time of testing (see "CSH Model").

Open-Field Activity

Spontaneous open-field behavior was evaluated in mice from both rearing groups at P16–P18 and at P40–P45. CSH ($n = 28$) and control ($n = 21$) mice tested between P16 and P18 were placed in a Plexiglas enclosed open field (25 × 25 × 40 cm) equipped with infrared photo beams coupled to a computer running TruScan software (Coulbourn Instruments, Whitehall, PA) to automatically record both horizontal and vertical movements within the field. Activity was monitored during a single 12-min session and measures of total distance moved, center distance, the average velocity of movements, rest time, and center time were recorded. Data were binned into three 4-min intervals for statistical analysis. CSH ($n = 12$) and control ($n = 13$) mice tested between P40 and P45 were monitored for open-field activity in a similar way, with the exception that the Plexiglas chamber was larger (41 × 41 × 40 cm) and the length of the session was increased to 15 min to compensate for the increased mobility and size of the animals. Data for this older group were binned into three 5-min intervals for statistical analysis. Data were analyzed using a multivariate ANOVA with repeated measures.

Spatial-Delayed Alternation

Using an automated Y-maze we tested CSH ($n = 11$) and control ($n = 13$) mice on a delayed alternation spatial memory task. Mice between P45 and P60 were maintained on a 22-h deprivation schedule in which they had ad libitum access to food for only 2 h each day, followed by 22 h of food deprivation. Mice had unlimited access to water at all times. The 2 h of access to food occurred immediately following each day's testing session. Mice were trained to retrieve highly palatable and reinforcing chocolate sprinkles from food cups placed at the ends of the 2 choice arms of the Y-maze. The distance between the food cups at either end of the choice arms of the maze and the choice point in the start box was 42 cm. Chocolate sprinkles with a hard coating were used to minimize the potential for olfactory cues being used to perform the task. Mice initially underwent a shaping procedure to retrieve the reinforcements from the food cups. After sufficient shaping, mice were tested on the delayed alternation task for 10 trials per day until they reached a criterion performance of 80% correct responses over 2 successive test sessions at a given delay or failed to reach criterion performance within 200 trials. Successful learning of the task required that animals alternate the arm entered after retrieving the reinforcement on the previous trial from the opposite arm. After reaching criteria on the task with no delay, a 25-s delay was introduced between being placed in the start box and the opportunity to make the next choice. Following completion of the task with a 25-s delay, the delay interval was increased to 1 min and then 5 min. Criterion performance at each delay advanced the animal on to the next delay interval. Failure to reach criterion within 200 trials terminated testing and the animal was not tested at the next longer delay. The initial trial of each session consisted of baiting both arms of the Y-maze and recording the arm selected by the animal. Thereafter, only a single arm was baited. The baited arm for each trial was the arm opposite to the arm selected on the last reinforced choice. Successful learning of the task required that the mice remember the arm selected on the previously reinforced trial and to choose to enter the opposite arm on the next trial. Following each trial, an intertrial interval or delay was interposed during which the mouse was placed in the start arm with an opaque door separating the mouse from the choice arms of the maze. During this time the common portion of the maze connecting the 3 arms was wiped with 50% alcohol to prevent the use of odor cues in guiding the response of the animal during the next trial. The statistical analysis of delayed alternation task data was performed using a time-to-event product–limit log rank test to compare the curves for trials to criteria (Friedman et al. 1998) and number of animals failing to reach criteria in 200 trials (SPSS, Inc., Chicago, IL).

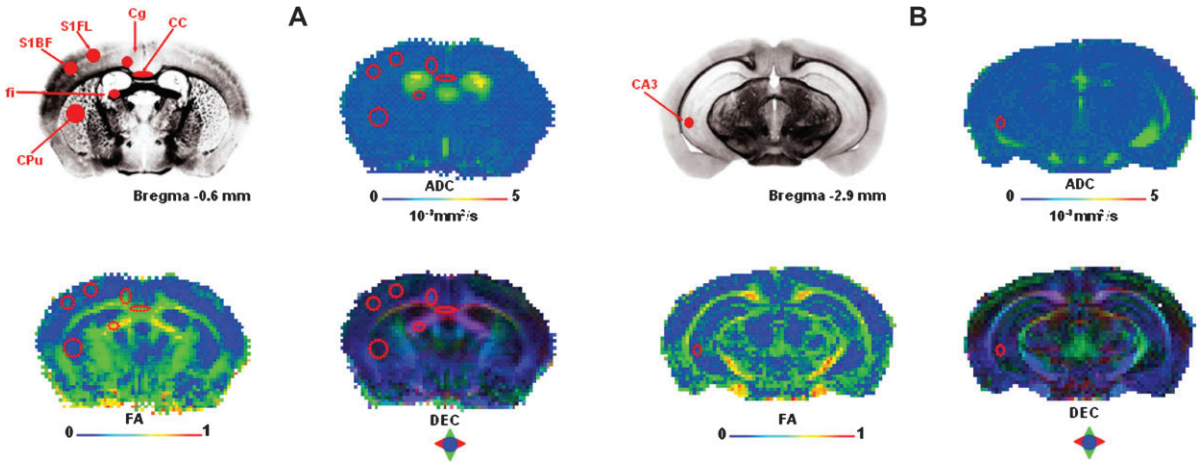

Figure 1. Depiction of ROIs in DTI data. Representative ROIs in (*A*) anterior and (*B*) posterior coronal slices located approximately −0.6 and −2.9 mm relative to bregma from a C57B/L6 mouse brain atlas (Sidman et al (http://www.hms.harvard.edu/research/brain/atlas.html)). Approximate locations and sizes of the ROIs for corpus callosum (CC), cingulum (Cg), caudate putamen (CPu), fimbria (fi), and field CA3 (CA3) of the hippocampus, and primary somatosensory areas of the forelimb (S1FL) and whisker barrel field (S1BF) are shown (top left). Placement of ROIs is also shown in DTI maps (voxel size of 156 × 156 × 500 μm) of a P38 control mouse demonstrating maps of ADC (top right), FA (bottom left), and DEC maps (bottom right).

Free-Swim Test

Nine control and 7 CSH mice were tested at 4 months of age. Briefly, mice were placed in the center of a tank of water with a depth of 33 cm and measuring 33 cm in diameter. They were allowed to free swim for 5 min while being video recorded by an overhead camera. Three 5-min sessions were given with an intersession interval of approximately 48 h. Videotape records of the swimming activity were analyzed by placing a transparent overlay with 30° axes over the video image of the tank. A rightward (clockwise) or leftward (counter-clockwise) turn was scored when the subject actively swam across 30°. A record of the total number of turns, number of turns in each direction, and the preferred direction of turns over each 5-min session was recorded. Degree of laterality was scored as the percent of the total number of turns that were in the preferred direction and consistency of laterality (preferred direction) across sessions was also calculated. Data were analyzed using a MANOVA test with repeated measures.

Results

Figure 1 provides the locations of the ROIs sampled in different brain areas and depicts the representative in vivo DTI parametric maps from control mice at near constant temperature (~37 °C) and normal physiology. The ADC maps represent the degree of mobility of water protons in the tissue. The FA maps represent differences between gray and white matter and provides information about tissue organization. The DEC maps reflect orientation-specific anisotropies in the medial–lateral, dorsal–ventral, and anterior–posterior directions with R, G, and B colors, respectively. In the DEC map, the intensity of each color reflects the degree of anisotropy in that given direction and therefore the intensity is the same as the FA map. In addition, axial ($\lambda_{\parallel}$) and radial ($\lambda_{\perp}$) water diffusivities were used to qualitatively provide measures of intact fibers and lack of myelin.

Age-Dependent DTI Parameters

Student's *t*-tests were performed at each age group to signify differences of DTI parameters between CSH and control mice. Developmental profiles of diffusion anisotropy differed between control and CSH mice in some (corpus callosum, cingulum, fimbria of hippocampus) but not other (somatosensory cortex, caudate putamen, CA3 field of hippocampus) regions.

For example, as shown in Figure 2*A,B* for corpus callosum and cingulum respectively, FA changes during maturation were significantly different between control and CSH mice. For control mice, FA increased over the period between P15 and P51 in both of these regions. CSH mice also exhibited increasing FA over the same period, but at each age group the FA values in CSH mice were consistently lower than in control mice. The differences in FA between control and CSH mice reached statistically significant levels at P45 ($P < 0.02$ in corpus callosum; $P < 0.05$ in cingulum) and P51 ($P < 0.01$ in corpus callosum; $P < 0.002$ in cingulum). These FA changes had directional dominance, as shown in Figures 2*C,D* for corpus callosum and cingulum respectively. From the respective DEC maps, it was found that in the corpus callosum the anisotropy was dominant in the medial–lateral direction (i.e., R color map), whereas in the cingulum the anisotropy was dominant in the anterior–posterior direction (i.e., B color map). The maturational profiles for control and CSH mice with respect to directional anisotropy were similar to the FA changes, but statistical analysis by ANOVA revealed that the linear developmental trend in the medial–lateral direction for corpus callosum ($P < 0.0015$) and the anterior–posterior direction for cingulum ($P < 0.0016$) were significantly different in CSH mice compared with control mice.

These developmental trends in FA could be visualized in individual subject data, specifically when comparing DTI images from early (P15) versus late (P51) in development. An example of the reduction in FA for the corpus callosum and cingulum of CSH mice compared with control mice is shown in Figure 3*A*. Examples of reductions in directional anisotropy in medial–lateral direction for corpus callosum and the anterior–

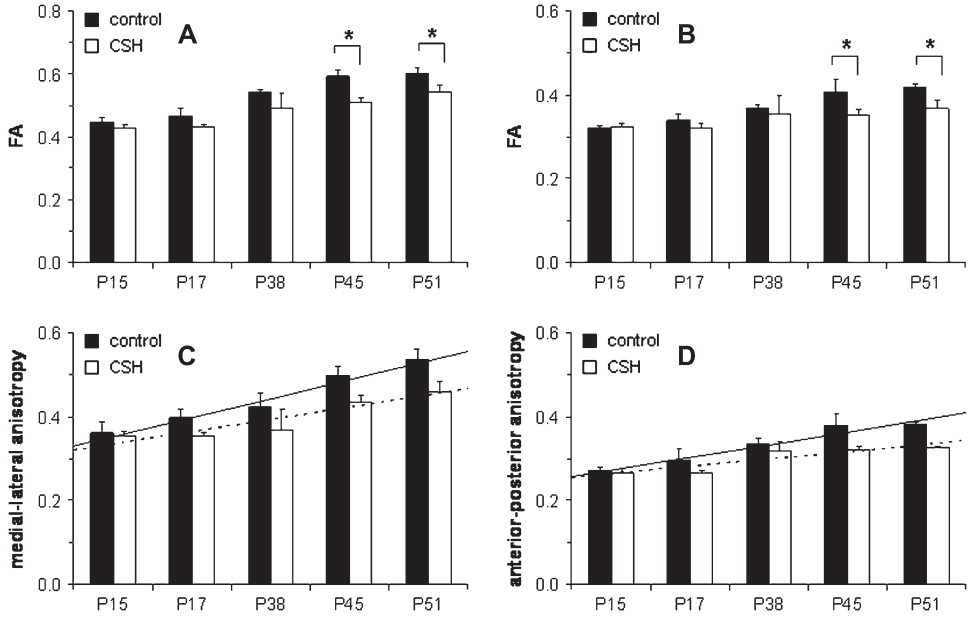

Figure 2. Developmental profile of FA (top) and directional anisotropy (bottom) for control and CSH mice. Changes in FA in (*A*) corpus callosum and (*B*) cingulum for control (black) and CSH (white) mice. FA values increased over development, but in CSH mice the values were reduced throughout maturation. There were significant differences in FA values between control and CSH mice at P45 ($P < 0.02$ in *A*; $P < 0.05$ in *B*) and P51 ($P < 0.01$ in *A*; $P < 0.002$ in *B*). Changes in anisotropy in terms of (*C*) medial–lateral direction in corpus callosum and (*D*) anterior–posterior direction in cingulum for control (black) and CSH (white) mice. The linear developmental trajectory at the medial–lateral ($P < 0.0015$, ANOVA) and anterior–posterior ($P < 0.0016$, ANOVA) anisotropy values for control mice (solid line) were significantly different from CSH mice (dotted line).

posterior direction for cingulum are shown in Figure 3*B*,*C*, respectively. Similar to the group (Fig. 2) and individual (Fig. 3) data for corpus callosum and cingulum revealing the hypoxia-induced anisotropy decreases, Figure 4 shows DTI data from fimbria of hippocampus, where the FA differences between control and CSH mice were significant at both P15 ($P < 0.02$) and P51 ($P < 0.04$).

Developmental profiles of diffusion anisotropy in other regions were not significantly different between CSH and control mice (data not shown). FA in gray matter areas of the somatosensory cortex (Fig. 1*A*) and the CA3 field of hippocampus all revealed insignificant differences between CSH and control mice or for maturation-based changes. However, we note that location of the ROI for field CA3 of hippocampus near the ventricles (Fig. 1*B*) makes this region quite difficult for quantification. No significant differences were found between CSH and control mice for FA in the caudate putamen. Although control mice displayed a significant increase in FA between P15 and P51 (0.07 ± 0.06 to 0.22 ± 0.01) that was most pronounced in the anterior–posterior and dorsal–ventral directions (Chahboune et al. 2007), we did not observe any significant maturation-based FA changes in the caudate putamen of CSH mice.

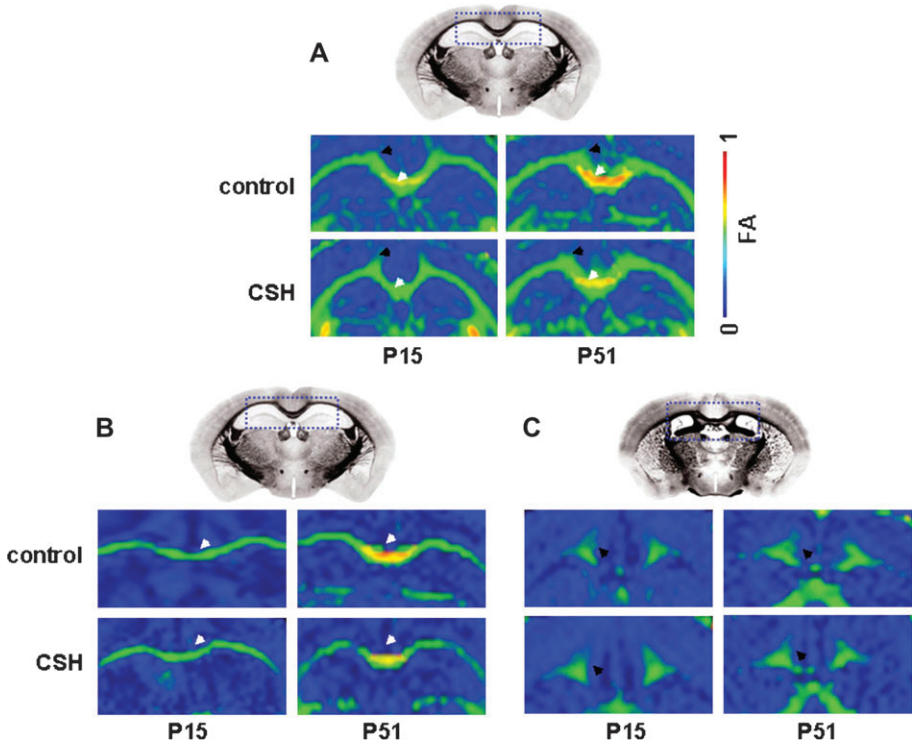

Figure 3. Representative DTI data of control and CSH mice at P15 and P51 emphasizing the anisotropy differences in corpus callosum (white arrow) and cingulum (black arrow). (*A*) FA maps show that older (P51) CSH mice exhibit significantly lower FA values than those of age-matched controls, whereas younger (P15) CSH mice exhibit similar FA values compared with those of age-matched controls. Anisotropy maps of (*B*) medial-lateral direction in corpus callosum and (*C*) anterior–posterior direction in cingulum show that in older (P51) CSH mice exhibit significantly lower anisotropy values than those of age-matched controls, whereas younger (P15) CSH mice exhibit similar anisotropy values compared with those of age-matched controls. DTI data from individual subjects, whereas the reference images were obtained from Sidman et al. (http://www.hms.harvard.edu/research/brain/atlas.html).

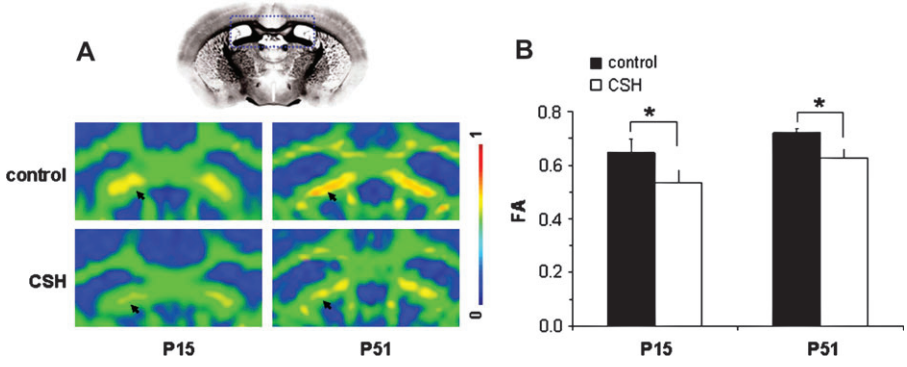

Figure 4. DTI data of control and CSH mice at early (P15) and late (P51) in development emphasizing FA differences in fimbria of the hippocampus. CSH mice exhibited lower FA values compared with their age-matched control. (*A*) FA values were lower in CSH mice than in their age-matched controls as observed in DTI data from individual subjects. The reference image was obtained from Sidman et al (http://www.hms.harvard.edu/research/brain/atlas.html). (*B*) Group average FA values were significantly lower in CSH mice than in their age-matched controls, both in early ($P < 0.02$) and late ($P < 0.04$) in development.

In control mice, ADC values underwent a small but statistically significant ($P < 0.01$) developmental decrease in the corpus callosum (i.e., 0.8×10^{-3} to 0.5×10^{-3} mm^2/s), cingulum (i.e., 0.8×10^{-3} to 0.5×10^{-3} mm^2/s), fimbria of hippocampus (i.e., 0.9×10^{-3} to 0.8×10^{-3} mm^2/s), the CA3 field of hippocampus (i.e., 0.8×10^{-3} to 0.7×10^{-3} mm^2/s), whisker barrel field (i.e., 0.7×10^{-3} to 0.6×10^{-3} mm^2/s) and forelimb (i.e., 0.7×10^{-3} to 0.5×10^{-3} mm^2/s) areas of the somatosensory cortex between P15 and P51. ADC values in the caudate putamen were generally stable throughout normal adolescence. In CSH mice, however, only slight and non-significant changes in ADC values were observed in these same areas. Examination of the ADC maps, which reveals good contrast between cerebral spinal fluid and brain tissue, showed no ventriculomegaly in CSH mice at any time points, from P15 to P51. The observed ADC trends over normal development are in general agreement with our prior results (Chahboune et al. 2007), and the absence of hypoxia-induced ventriculomegaly is in agreement with our previous results indicating a recovery for measures of brain weight, cortical volume and ventriculomegaly within 7 days following removal from hypoxia (Fagel et al. 2006).

Radial diffusivity maps ($\lambda_\perp$) generally followed the trends of the ADC maps—that is, a statistically significant developmental decrease in control mice (data not shown). Because the axial diffusivity ($\lambda_{||}$) is a few times greater than its radial counterpart, we examined hypoxia-induced differences early (P15) and late (P51) in development. The same regions depicting FA changes between CSH and control mice (i.e., corpus callosum, cingulum, fimbria of hippocampus; Figs 2–4) revealed slightly reduced values of $\lambda_{||}$ in CSH mice, both early and late in development (Table 1).

Locomotor Activity, Spatial Memory, and Behavioral Laterality

Analysis of open-field activity for CSH mice between P16 and P18 revealed an elevated pattern of general activity compared with controls (Table 2). On measures of total distance traveled ($F_{1,47} = 5.3$, $P = 0.02$), time spent in the center of the open field ($F_{1,47} = 3.9$, $P = 0.05$), and the average velocity of movements ($F_{1,47} = 9.1$, $P = 0.004$) CSH mice had significantly elevated values, while the amount of time spent not moving (rest time) was significantly decreased ($F_{1,47} = 5.0$, $P = 0.03$). In contrast to the pattern of elevated activity found early in development, assessment of open-field behavior between P40 and P45 revealed no significant differences between control and CSH mice on the same measures (Table 3).

Assessment of spatial memory using the delayed alternation task revealed significant differences between control and CSH mice when testing began between P45 and P60. Using a time-to-event product-limit log rank test (Friedman et al. 1998) to compare the curves for trials to criteria and failure rates for CSH and control mice at the 25-s delay revealed no significant difference in performance (Table 4; Fig. 5*A*, $P < 0.8388$). CSH mice tested with 1-min (Table 4; Fig. 5*B*, $P < 0.0485$) and 5-min (Table 4; Fig. 5*C*, $P < 0.0218$) delays required significantly more trials to criterion than did control mice and a greater number of the CSH mice failed to reach criterion prior to the 200 trial cut-off on the 5-min delay. These data indicate that while CSH mice are capable of performing spatial memory tasks over short periods of time, when required to hold this information "online" for more prolonged periods, CSH mice exhibit profound deficits in spatial memory.

Analysis of the degree of behavioral laterality using the free-swim task revealed lasting differences between CSH and control mice for the total number of turns per session (Table 5; $F_{1,14} = 5.2$, $P = 0.038$) and the laterality of turns (Table 5; $F_{1,14} = 5.5$, $P = 0.035$). Assessing the consistency of the preferred direction of turns across sessions also revealed a significant difference, with 7 of 9 control mice maintaining the same directional preference across all 3 sessions while only 1 of 7 CSH mice were consistent across sessions (Table 5; $F_{1,14} = 9.2$, $P = 0.09$). These data indicate that CSH mice exhibit less behavioral lateralization and less consistency of lateralized behavior than do age-matched mice reared under normal conditions. In addition, the assessment of these behaviors at 4 months of age reveals that these differences are long lasting and are not significantly modified by exposure to a normal environment after the early period of hypoxia.

Discussion

We used in vivo DTI to examine the organization of selected brain regions during early postnatal development and their sensitivity to morphological change as a result of exposure to chronic hypoxia during the early postnatal period. Hypoxia affected the maturation of some white matter regions (corpus callosum, cingulum, fimbria of hippocampus) by stunting developmental changes, from P15 to P51, as well as the final level of anisotropy of these axonal pathways. Sampled areas of gray matter in control and CSH mice showed negligible or modest differences in DTI parameters during this period. In addition, the results from our analysis of activity and cognitive behaviors provided some functional correlates for the white matter injuries identified in CSH mice. Because the CSH model mimics the effects of preterm birth, we believe that the results may have clinical relevance.

Developmental Changes in DTI Parameters

We observed significant changes in several DTI parameters for white matter pathways over the developmental period of P15

Table 1
Water diffusivity parallel to axonal fiber tracts ($\lambda_{||}$ in units of $\times 10^{-3}$ mm^2/s) of control and CSH mice

	Corpus callosum		Cingulum		Fimbria of hippocampus	
	P15	P51	P15	P51	P15	P51
Control	1.29 ± 0.01	1.31 ± 0.01	1.02 ± 0.01	1.00 ± 0.01	1.60 ± 0.02	1.69 ± 0.01
CSH	1.21 ± 0.01	1.24 ± 0.01	0.97 ± 0.01	0.92 ± 0.01	1.41 ± 0.01	1.51 ± 0.01
P values	<0.05	<0.05	<0.09	<0.05	<0.004	<0.01

Note: Summary of $\lambda_{||}$ values in the corpus callosum, cingulum and fimbria of hippocampus, at early (P15) and late (P51) in development. Results show that $\lambda_{||}$ values were lower in CSH mice than in their age-matched controls in all regions, however the differences were far more significant in corpus callosum and the fimbria of the hippocampus.

Table 2
Results of open-field activity early in development (P16–P18) for control and CSH mice

	Total distance (cm)	Velocity (cm/min)	Rest time (s)	Center time (s)
Control ($n = 21$)	1445 ± 144	115 ± 10.8	383 ± 24.9	102 ± 19.5
CSH ($n = 28$)	‡1889 ± 125.4	†158 ± 9.4	‡309 ± 21.6	‡153 ± 16.2

Note: Measures of total distance traveled, average velocity of movements, average rest time, and time spent in the center of the open field. While the amount of time spent not moving (i.e., rest time) was significantly decreased in CSH mice compared with their age-matched controls, all other measures showed hyperactivity ($^{\ddagger}P < 0.05$, $^{\dagger}P < 0.01$).

Table 3
Results of open-field activity late in development (P40–P45) for control and CSH mice

	Total distance (cm)	Velocity (cm/min)	Rest time (s)	Center time (s)
Control ($n = 13$)	4500 ± 240	305 ± 14.4	286 ± 10.5	240 ± 24.1
CSH ($n = 12$)	4524 ± 250	301 ± 15.0	285 ± 10.8	237 ± 25.2

Note: Measures of total distance traveled, average velocity of movements, average rest time, and time spent in the center of the open field. All behavioral measures showed no significant differences between CSH mice compared with their age-matched controls.

Table 4
Results of spatial-delayed alternation test (Y-maze) for control and CSH mice, late in development (P45–P60)

	Mean trials to criteria	% Mice not reaching criteria after 200 trials
Control—25-s delay	64	0
CSH—25-s delay	71	0
Control—1-min delay	51	0
CSH—1-min delay	110‡	0
Control—5-min delay	119	31%
CSH—5-min delay	180†	73%

Note: Mean trials to criteria and percentage of animals failing to reach criteria after 200 trials on delayed alternation task with 25-s, 1- and 5-min delays. Time-to-event statistics revealed that control ($n = 13$) versus CSH ($n = 11$) mice differed significantly at the 1 min ($^{\ddagger}P < 0.0485$) and 5 minute ($^{\dagger}P < 0.0218$) delays. See also Figure 5.

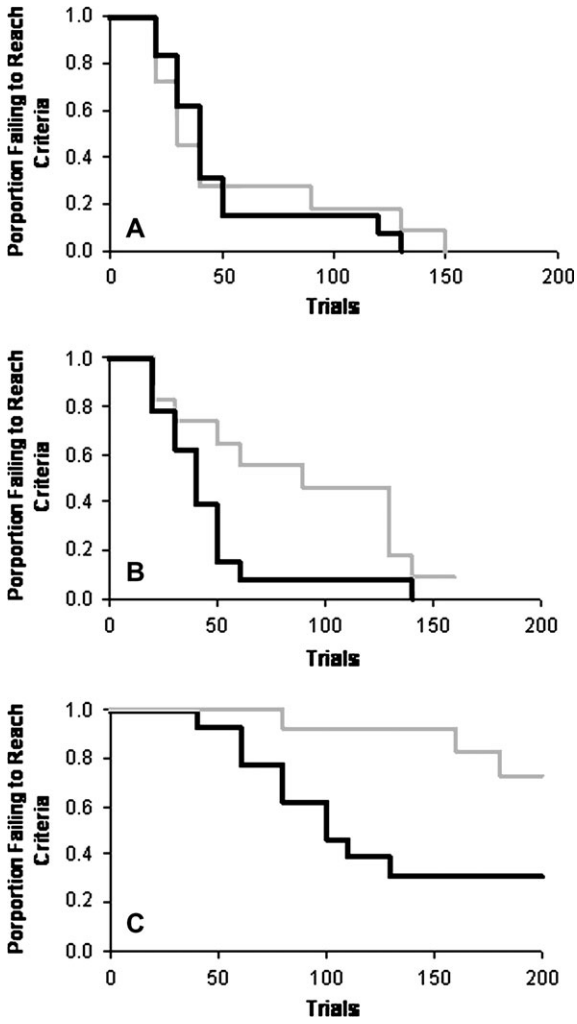

Figure 5. Results of the spatial-delayed alternation test (Y-maze) for control (black line) and CSH mice (gray line) for delay intervals of (*A*) 25 s, (*B*) 1 min, and (*C*) 5 min, late in development (P45–P60). Graph lines indicate the proportion (vertical axis) of animals within each group failing to reach criterion performance (80% correct responses in 2 consecutive daily sessions) versus the number of trials needed to reach criterion (horizontal axis). No significant difference was found in the trials to reach criteria performance or in the number of animals failing to reach criteria within 200 trials with the 25-s delay (*A*). However, CSH and control mice were significantly different in the trials to criteria and the number of animals failing to reach criteria in 200 trials for both the 1-min (*B*; $P < 0.0485$) and 5-min delays (*C*; $P < 0.0218$). See also Table 4.

Table 5
Results of free-swim task for control and CSH mice, quite late in development (~4 months)

	Mean turns per session	Laterality (% turns in preferred direction)
Control ($n = 9$)	268.5	84.1%
CSH ($n = 7$)	‡126.8	‡71.6%

Note: Measures of turns made per session during a free-swim task and turns made in the preferred direction (i.e., laterality). Both behavioral measures showed significant differences between CSH mice compared with their age-matched controls ($^{\ddagger}P < 0.03$).

to P51 in control mice. FA values increased over this period within each of the pathways examined. Our data indicate that the corpus callosum had the highest FA value of any of the areas sampled and that this organizational feature emerges as early as P15. The early appearance of this high level of coherent parallel organization, at the earliest ages is consistent with a lack of divergent trajectories by callosal axons within this midline pathway even at stages prior to complete myelination (Vincze et al. 2008). In contrast to the corpus callosum, FA values in the cingulum were lower throughout the developmental period examined. The reduced directional anisotropy within the cingulum (anterior–posterior) compared with the corpus callosum (medial–lateral) may reflect a greater divergence of fiber trajectories within this pathway resulting from fibers entering and exiting from overlying cortical and subcortical areas (Barkovich 2000). The ADC (and $\lambda_{\perp}$) decreases were apparent in both gray matter and white matter with age. However the water diffusivity in white matter was higher than in gray matter early in development, reflecting a greater tissue volume of water with less cell compactness and membrane content. The ADC maps revealed the absence of ventriculomegaly in hypoxic mice as early as P15 consistent with our earlier study demonstrating the rapid reversal of the hypoxia-induced abnormalities in ventricular and cortical volumes within 7 days of the cessation of the hypoxia at P11 (Fagel et al. 2006).

The developmental changes in FA values for regions of the corpus callosum, cingulum, and fimbria of hippocampus in control mice can be attributed to various factors. Myelin may play a role in modulating the degree of anisotropy, yet may not be sufficient or necessary for expressing the anisotropic changes. Studies in animals show a similar level of anisotropy in the unmyelinated olfactory nerve as the anisotropy found in the myelinated trigeminal and optic nerves of the garfish (Beaulieu and Allen 1994). These results illustrate the important role played by axonal membranes, exclusive of myelin, in determining levels of anisotropy within some fiber pathways. Other studies in rodents have also reported high anisotropy in premyelinated embryonic and neonatal brains (Mori et al. 2001; Zhang et al. 2003). The changes in the cellular composition of white matter structures, which include increase in the number of microtubule-associated proteins in axons, a change in axon caliber, and a significant increase in the number of oligodendrocytes could explain, in part, the expression of the FA (Huppi and Dubois 2006). Other factors intrinsic to the axon could also contribute to the production of anisotropy, for example, changes in fiber diameter, neurofilament development, extracellular–intracellular matrix, and sodium channel activity (Waxman et al. 1989; Prayer et al. 2001; McGraw et al. 2002; Beaulieu 2006; Mori et al. 2006).

Effects of Hypoxia on DTI Parameters

The most striking difference between CSH and control mice in our quantitative diffusion measurements of white matter fiber tracts was the significantly lower anisotropy values in the corpus callosum, cingulum, and fimbria of the hippocampus in the CSH mice. The reductions in FA are likely to result from reduced water diffusivity for the axons of these pathways. In accord with this view, we found reduced axial diffusivity ($\lambda_{\|}$) in these regions of CSH mice between P15 and P51, potentially reflecting damage to the axons as $\lambda_{\|}$ is believed to represent parallel water diffusivity within intact axonal fibers in white matter of mammalian brains (Song et al. 2002, 2003). The hypoxia-induced lower $\lambda_{\|}$ value may also be consistent with a disturbance in the development of the axonal trajectories of these fibers. Studies suggest that hypoxia is associated with axonal degeneration, axon sprouting, and arrested oligodendrocyte lineage (Hu and Strittmatter 2004). These events all play an important role in both fiber tract alignment and packing (Rasband et al. 1999; Drobyshevsky et al. 2005). Clinically, misrouted fiber trajectories have also been documented using DTI in a hypoxia model of brain insult in prematurely delivered children (Huppi et al. 2001; Fan et al. 2006). The reduction of FA and directional anisotropy correlate with histological alterations in the brains exposed to hypoxia challenge. The decreased FA value of the corpus callosum, cingulum, and fimbria of hippocampus can be ascribed to several deficits in CSH mice. In mice reared under identical conditions to those used in the present study, we have previously described changes in myelin, the size of developing fiber pathways, decrease of neuronal number, and connectivity or alterations in axonal membrane-associated skeletal protein (Curristin et al. 2002; Westin et al. 2002; Back et al. 2006; Fagel et al. 2006).

Compared with the major axonal pathways of the corpus callosum, cingulum, and fimbria of the hippocampus, no maturation-based changes were found for FA values in the gray matter areas of the hippocampus or the forelimb and whisker areas of the somatosensory cortex, in either CSH or control mice between P15 to P51. These data are consistent with previous studies of mouse brain that have reported that FA values in these regions do not vary significantly after P10 (Verma et al. 2005; Chahboune et al. 2007). In the immature brain, white matter appears more vulnerable to hypoxia than gray matter, with the white matter being selectively damaged by exposure to hypoxia. This pathogenesis has been related to various factors, including regional differences in vasculature, autoregulatory responses, excitatory receptors, and the higher susceptibility of late oligodendrocyte progenitors to hypoxia in periventricular white matter (Follett et al. 2000; Rezaie and Dean 2002; Volpe 2003; McQuillen and Ferriero 2004).

Impact of Hypoxia on Behavior

Previous studies investigating the impact of hypoxia on open-field behavior in neonatal rats are consistent with the transient nature of hyperactivity we observed in CSH mice (Dell'Anna et al. 1991; Iuvone et al. 1996; Speiser et al. 1998). Interestingly, the elevated levels of activity observed in both mice and rats at P16–18 are normalized by P45, at a time prior to when we first identified significant differences in anisotropy values between control and CSH mice. The disparity in timing of these events makes it unlikely that the transient hyperactivity that results from neonatal hypoxic exposure is a consequence of the observed differences in the maturational profile or directional organization of axons within the corpus callosum, cingulum, or fimbria of hippocampus. The lack of correlation between the expression and subsequent normalization of hyperactivity in CSH mice and the timing of alterations we have identified for DTI measures of white matter structures suggests that the alterations in the maturation and organization of these connectional pathways are an unlikely substrate for early expression of hyperactivity. We have previously shown that cortical neurons, including interneurons, undergo a significant decrease in number during hypoxia and that following the return to a normoxic environment at P11 total neuron number recovers to normal levels by P49 (Fagel et al. 2006). Additionally, Muller Smith et al. (2008) has demonstrated that cortical interneurons play an important role in the expression of hyperactivity in FGF receptor knockout mice. Thus, it may be the hypoxic induced changes in this inhibitory population of cells and not the projections of primary neurons that underlie the expression of hyperactivity in CSH mice early in development.

In contrast to the transient nature of differences in open-field behavior between CSH and control mice, analysis of spatial memory abilities with the delayed alternation task revealed a lasting and profound impairment present at the time when FA differences are significant within the corpus callosum, cingulum, and fimbria of hippocampus. The ability of both CSH and control mice to acquire and perform this spatial memory task with moderate delay periods indicates that they do not have a fundamental deficit in basic spatial information processing or in maintaining memory for this type of information over limited periods of time. However as the length of time required to retain this information increased, the CSH mice exhibited profound performance deficits. The CA3 field of the hippocampus and its output via the fimbria has been shown to be important substrates for the type of short term spatial memory encoding required by the delayed alternation task (Kesner

2007). Lesions of the fimbria of the fornix in rats results in significant delay dependent deficits in spatial memory (Markowska et al. 1989). The deficits in this task at long delays are also consistent with the deficits observed in mice with prefrontal cortical lesions with increasing delays on radial arm maze tasks (Touzani and Sclafani 2007). Therefore, the alterations in cortical neuron number (Fagel et al. 2006) and hippocampal related outputs, such as the fimbria of the hippocampus may play an important role in the spatial memory deficits found in CSH mice. Examination of the persistence of the FA differences between CSH and control mice performed in conjunction with the testing of delayed alternation performance at later ages may provide further insight into the relationship of these defects in structure and function.

Consistent with the profound and lasting impairment in spatial memory abilities identified with the delayed alternation task, our results using the free-swim task also point to lasting alterations of behavioral laterality in CSH mice. Previous studies using the free-swim task indicate that variations in rotational preference and lateralization are linked to patterns of callosal connectivity. For example, mice with callosal agenesis or transection of the corpus callosum exhibit greater laterality in this task than normal mice (Filgueiras and Manhaes 2004, 2005). Further, the earlier the age of callosal alteration, the greater the impact on long-term laterality (Manhaes et al. 2007). These data coupled with the differences between CSH and control mice on callosal maturation and organization revealed by our DTI studies suggest that early hypoxia exposure may have a significant impact on long-term hemispheric asymmetries and behavioral lateralization. In contrast to the pattern of increased laterality observed in mice lacking, or with diminished, callosal connectivity (Filgueiras and Manhaes 2004, 2005), mice reared under hypoxic conditions exhibit a reduction in the expression and consistency of laterality. These data suggest that not only is the presence of hemispheric connection important for the manifestation of behavioral asymmetries, but also that the pattern and organization of connectivity may play an important role in the expression of behavioral asymmetries. Finally, it remains to be determined if the modification of lateralization requires long lasting changes in the organization of callosal connectivity, or whether disruption or delay of the normal sequence of callosal maturation is sufficient to produce the lasting alterations we have identified.

Summary

Understanding the consequences of neonatal hypoxia on behavioral outcome and connectivity using DTI may provide important clues for understanding the neurodevelopmental difficulties affecting very low birth weight preterm infants. In this study, we have demonstrated that hypoxia has a profound effect on the temporal maturation and organization of several major connectional pathways related to the cerebral cortex and hippocampus. Alterations in these pathways in CSH mice are consistent with the types of functional impairments in spatial working memory and behavioral asymmetries that we have observed following early hypoxic exposure in mice. As exposure to an enriched environment may increase the size or number of axons in the corpus callosum and improve performance in several memory and learning tasks in rats, in future experiments we could perform longitudinal studies with DTI to test whether alterations in experience, such as exposing hypoxic mice to an enriched environment, also results in observable changes in white matter structures.

Funding

National Institutes of Health grants (R01 MH-067528, R01 DC-003710, P30 NS-52519, P01 NS-35476); and a gift from Pfizer.

Notes

We thank Peter Brown and Xiaoxian Ma for engineering and surgical help, Dr Robert Makuch and Karol Katz for statistical help on the behavioral studies, and Jacob Kravitz and Weili Yan for behavioral testing of mice. *Conflict of Interest*: None declared.

Address correspondence to Fahmeed Hyder, PhD, Department of Diagnostic Radiology, Yale University, N143 TAC, 300 Cedar Street (MRRC), New Haven, CT 06510, USA. Email: fahmeed.hyder@yale.edu.

References

Back SA, Craig A, Luo NL, Ren J, Akundi RS, Ribeiro I, Rivkees SA. 2006. Protective effects of caffeine on chronic hypoxia-induced perinatal white matter injury. Ann Neurol. 60:696–705.

Barkovich AJ. 2000. Concepts of myelin and myelination in neuroradiology. Am J Neuroradiol. 21:1099–1109.

Bassan H, Feldman HA, Limperopoulos C, Benson CB, Ringer SA, Veracruz E, Soul JS, Volpe JJ, du Plessis AJ. 2006. Periventricular hemorrhagic infarction: risk factors and neonatal outcome. Pediatr Neurol. 35:85–92.

Basser PJ. 1995. Inferring microstructural features and the physiological state of tissues from diffusion-weighted images. NMR Biomed. 8: 333–344.

Basser PJ, Mattiello J, LeBihan D. 1994. MR diffusion tensor spectroscopy and imaging. Biophys J. 66:259–267.

Basser PJ, Pajevic S. 2003. A normal distribution for tensor-valued random variables: applications to diffusion tensor MRI. IEEE Trans Med Imaging. 22:785–794.

Beaulieu C, Allen PS. 1994. Determinants of anisotropic water diffusion in nerves. Magn Reson Med. 31:394–400.

Beaulieu C. 2006. The biological basis of diffusion tractography. IEEE Biomed Imaging: Macro to Nano. 1–3:347–350.

Boardman JP, Counsell SJ, Rueckert D, Hajnal JV, Bhatia KK, Srinivasan L, Kapellou O, Aljabar P, Dyet LE, Rutherford MA, Allsop JM, Edwards AD. 2007. Early growth in brain volume is preserved in the majority of preterm infants. Ann Neurol. 62:185–192.

Boska MD, Hasan KM, Kibuule D, Banerjee R, McIntyre E, Nelson JA, Hahn T, Gendelman HE, Mosley RL. 2007. Quantitative diffusion tensor imaging detects dopaminergic neuronal degeneration in a murine model of Parkinson's disease. Neurobiol Dis. 26:590–596.

Budde MD, Kim JH, Liang HF, Russell JH, Cross AH, Song SK. 2007. Axonal injury detected by in vivo diffusion tensor imaging correlates with neurological disability in a mouse model of multiple sclerosis. NMR Biomed. 57:688–695.

Chahboune H, Ment LR, Stewart WB, Ma X, Rothman DL, Hyder F. 2007. Neurodevelopment of C57B/L6 mouse brain assessed by in vivo diffusion tensor imaging. NMR Biomed. 20:375–382.

Curristin SM, Cao A, Stewart WB, Zhang H, Madri JA, Morrow JS, Ment LR. 2002. Disrupted synaptic development in the hypoxic newborn brain. Proc Natl Acad Sci USA. 99:15729–15734.

Dell'Anna ME, Calzolari S, Molinari M, Iuvone L, Calimici R. 1991. Neonatal anoxia induces transitory hyperactivity, permanent spatial memory deficits and CA1 cell density reduction in developing rats. Behav Brain Res. 45:125–134.

Dobbing J. 1972. Undernutrition and the developing brain. The relevance of animal models to the human problem. Bibl Nutr Diet. 17:35–46.

Drobyshevsky A, Derrick M, Prasad PV, Ji X, Englof I, Tan S. 2007. Fetal brain magnetic resonance imaging response acutely to hypoxia-ischemia predicts postnatal outcome. Ann Neurol. 61: 307–314.

Drobyshevsky A, Song SK, Gamkrelidze G, Wyrwicz AM, Derrick M, Meng F, Li L, Ji X, Trommer B, Beardsley DJ, Luo NL, Back SA, Tan S. 2005. Developmental changes in diffusion anisotropy coincide with immature oligodendrocyte progression and maturation of compound action potential. J Neurosci. 25:5988–5997.

Ennis DB, Kindlmann G. 2006. Orthogonal tensor invariants and the analysis of diffusion tensor magnetic resonance images. Magn Reson Med. 55:136–146.

Fagel DM, Ganat Y, Silbereis J, Ebbitt T, Stewart W, Zhang H, Ment LR, Vaccarino FM. 2006. Cortical neurogenesis enhanced by chronic perinatal hypoxia. Exp Neurol. 199:77–91.

Fan GG, Yu B, Quan SM, Sun BH, Guo QY. 2006. Potential of diffusion tensor MRI in the assessment of periventricular leukomalacia. Clin Radiol. 61:358–364.

Ferrer I, Soriano E, del Rio JA, Alcantara S, Auladell C. 1992. Cell death and removal in the cerebral cortex during development. Prog Neurobiol. 39:1–43.

Filgueiras CC, Manhaes AC. 2004. Effects of callosal agenesis on rotational side preference of BALB/cCF mice in the free swimming test. Behav Brain Res. 155:13–25.

Filgueiras CC, Manhaes AC. 2005. Increased lateralization in rotational side preference in male mice rendered acallosal by prenatal gamma irradiation. Behav Brain Res. 162:289–298.

Follett PL, Rosenberg PA, Volpe JJ, Jensen FE. 2000. NBQX attenuates excitotoxic injury in developing white matter. J Neurosci. 20:9235–9241.

Friedman LM, Furberg CD, DeMets DL. 1998. Fundamentals of clinical trials. New York: Springer-Verlag.

Gimenez M, Junque C, Narberhaus A, Botet F, Bargallo N, Mercader JM. 2006. Correlations of thalamic reductions with verbal fluency impairment in those born prematurely. Neuroreport. 17:463–466.

Guyer B, Hoyert DL, Martin JA, Ventura SJ, MacDorman MF, Strobino DM. 1999. Annual summary of vital statistics 1998. Pediatrics. 104:1229–1246.

Haddad GG, Jiang C. 1993. O2 deprivation in the central nervous system: on mechanisms of neuronal response, differential sensitivity and injury. Prog Neurobiol. 40:277–318.

Hasan KM, Basser PJ, Parker DL, Alexander AL. 2001. Analytical computation of the eigenvalues and eigenvectors in DT-MRI. J Magn Reson. 152:41–47.

Hu F, Strittmatter SM. 2004. Regulating axon growth within the postnatal central nervous system. Semin Perinatol. 28:371–378.

Huppi PS, Dubois J. 2006. Diffusion tensor imaging of brain development. Semin Fetal Neonatal Med. 11:489–497.

Huppi PS, Murphy B, Maier SE, Zientara GP, Inder TE, Barnes PD, Kikinis R, Jolesz FA, Volpe JJ. 2001. Microstructural brain development after perinatal cerebral white matter injury assessed by diffusion tensor magnetic resonance imaging. Pediatrics. 107:455–460.

Inder T, Neil J, Kroenke C, Dieni S, Yoder B, Rees S. 2005. Investigation of cerebral development and injury in the prematurely born primate by magnetic resonance imaging and histopathology. Dev Neurosci. 27:100–111.

Iuvone L, Geloso MC, Dell'Anna E. 1996. Changes in open field behavior, spatial memory, and hippocampal parvalbumin immunoreactivity following enrichment in rats exposed to neonatal anoxia. Exp Neurol. 139:25–33.

Jones DK, Horsfield MA, Simmons A. 1999. Optimal strategies for measuring diffusion in anisotropic systems by magnetic resonance imaging. Magn Reson Med. 42:515–525.

Kesner RP. 2007. Behavioral functions of the CA3 subregion of the hippocampus. Learn Mem. 14:771–781.

Laroia N, McBride L, Baggs R, Guillet R. 1996. Dextromethorphan ameliorates effects of neonatal hypoxia on brain morphology and seizure threshold in rats. Dev Brain Res. 100:29–34.

Manhaes AC, Abreu-Villaca Y, Schmidt SL, Filgueiras CC. 2007. Neonatal transection of the corpus callosum affects rotational side preference in adult Swiss mice. Neurosci Lett. 415:159–163.

Markowska AL, Olton DS, Murray EA, Gaffan D. 1989. A comparative analysis of the role of fornix and cingulate cortex in memory: rats. Exp Brain Res. 74:187–201.

Masutani Y, Aoki S, Abe O, Hayashi N, Otomo K. 2003. MR diffusion tensor imaging: recent advance and new techniques for diffusion tensor visualization. Eur J Radiol. 46:53–66.

Mazumdar A, Mukherjee P, Miller JH, Malde H, McKinstry RC. 2003. Diffusion-weighted imaging of acute corticospinal tract injury preceding Wallerian degeneration in the maturing human brain. AJNR Am J Neuroradiol. 24:1057–1066.

McGraw P, Liang L, Provenzale JM. 2002. Evaluation of normal age-related changes in anisotropy during infancy and childhood as shown by diffusion tensor imaging. AJR Am J Roentgenol. 179:1515–1522.

McQuillen PS, Ferriero DM. 2004. Selective vulnerability in the developing central nervous system. Pediatr Neurol. 30:227–235.

Mori S, Itoh R, Zhang J, Kaufmann WE, van Zijl PC, Solaiyappan M, Yarowsky P. 2001. Diffusion tensor imaging of the developing mouse brain. Magn Reson Med. 46:18–23.

Mori S, van Zijl PC. 1995. Diffusion weighting by the trace of the diffusion tensor within a single scan. Magn Reson Med. 33:41–52.

Mori S, Zhang J, Bulte JW. 2006. Magnetic resonance microscopy of mouse brain development. Methods Mol Med. 124:129–147.

Muller Smith K, Fagel DM, Stevens HE, Rabenstein RL, Maragnoli ME, Ohkubo Y, Picciotto MR, Schwartz ML, Vaccarino FM. 2008. Deficiency in inhibitory cortical interneurons associates with hyperactivity in fibroblast growth factor receptor 1 mutant mice. Biol Psychiatry. 63:953–962.

Nakada T, Matsuzawa H. 1995. Three-dimensional anisotropy contrast magnetic resonance imaging of the rat nervous system: MR axonography. Neurosci Res. 22:389–398.

Nosarti C, Giouroukou E, Healy E, Rifkin L, Walshe M, Reichenberg A, Chitnis X, Williams SC, Murray RM. 2008. Grey and white matter distribution in very preterm adolescents mediates neurodevelopmental outcome. Brain. 131:205–217.

Olavarria J, Van Sluyters RC. 1985. Organization and postnatal development of callosal connections in the visual cortex of the rat. J Comp Neurol. 239:1–26.

Pajevic S, Pierpaoli C. 1999. Color schemes to represent the orientation of anisotropic tissues from diffusion tensor data: application to white matter fiber tract mapping in the human brain. Magn Reson Med. 42:526–540.

Peterson BS, Vohr B, Staib LH, Cannistraci CJ, Dolberg A, Schneider KC, Katz KH, Westerveld M, Sparrow S, Anderson AW, Duncan CC, Makuch RW, Gore JC, Ment LR. 2000. Regional brain volume abnormalities and long-term cognitive outcome in preterm infants. JAMA. 284:1939–1947.

Prayer D, Barkovich AJ, Kirschner DA, Prayer LM, Roberts TP, Kucharczyk J, Moseley ME. 2001. Visualization of nonstructural changes in early white matter development on diffusion-weighted MR images: evidence supporting premyelination anisotropy. Am J Neuroradiol. 22:1572–1576.

Rasband MN, Peles E, Trimmer JS, Levinson SR, Lux SE, Shrager P. 1999. Dependence of nodal sodium channel clustering on paranodal axoglial contact in the developing CNS. J Neurosci. 19:7516–7528.

Reiss AL, Kesler SR, Vohr B, Duncan CC, Katz KH, Pajot S, Schneider KC, Makuch RW, Ment LR. 2004. Sex differences in cerebral volumes of 8-year-olds born preterm. J Pediatr. 145:242–249.

Rezaie P, Dean A. 2002. Periventricular leukomalacia, inflammation and white matter lesions within the developing nervous system. Neuropathology. 22:106–132.

Rothblat LA, Hayes LL. 1982. Age-related changes in the distribution of visual callosal neurons following monocular enucleation in the rat. Brain Res. 246:146–149.

Saigal S. 2000. Follow-up of very low birthweight babies to adolescence. Semin Neonatol. 5:107–118.

Saigal S, Doyle LW. 2008. An overview of mortality and sequelae of preterm birth from infancy to adulthood. Lancet. 371:261–269.

Schwartz ML, Vaccarino F, Chacon M, Yan WL, Ment LR, Stewart WB. 2004. Chronic neonatal hypoxia leads to long term decreases in the volume and cell number of the rat cerebral cortex. Semin Perinatol. 28:379–388.

Sizonenko SV, Camm EJ, Garbow JR, Maier SE, Inder TE, Williams CE, Neil JJ, Huppi PS. 2007. Developmental changes and injury induced disruption of the radial organization of the cortex in the immature rat brain revealed by in vivo diffusion tensor MRI. Cereb Cortex. 17:2609–2617.

Song SK, Kim JH, Lin SJ, Brendza RP, Holtzman DM. 2004. Diffusion tensor imaging detects age-dependent white matter changes in a transgenic mouse model with amyloid deposition. Neurobiol Dis. 15:640–647.

Song SK, Sun SW, Ju WK, Lin SJ, Cross AH, Neufeld AH. 2003. Diffusion tensor imaging detects and differentiates axon and myelin degeneration in mouse optic nerve after retinal ischemia. Neuroimage. 20:1714–1722.

Song SK, Sun SW, Ramsbottom MJ, Chang C, Russell J, Cross AH. 2002. Dysmyelination revealed through MRI as increased radial (but unchanged axial) diffusion of water. Neuroimage. 17:1429–1436.

Speiser Z, Katzir O, Rehavi M, Zabarski T, Cohen S. 1998. Sparing by rasagiline (TVP-1012) of cholinergic functions and behavior in the postnatal anoxia rat. Pharmacol Biochem Behav. 60:387–393.

Sun SW, Song SK, Harms MP, Lin SJ, Holtzman DM, Merchant KM, Kotyk JJ. 2005. Detection of age-dependent brain injury in a mouse model of brain amyloidosis associated with Alzheimer's disease using magnetic resonance diffusion tensor imaging. Exp Neurol. 191:77–85.

Thompson DK, Warfield SK, Carlin JB, Pavlovic M, Wang HX, Bear M, Kean MJ, Doyle LW, Egan GF, Inder TE. 2007. Perinatal risk factors altering regional brain structure in the preterm infant. Brain. 130:667–677.

Touzani K, Sclafani A. 2007. Insular cortex lesions fail to block flavor and taste preference learning in rats. Eur J Neurosci. 26:1692–1700.

Turner CP, Seli M, Ment L, Stewart W, Yan H, Johansson B, Fredholm BB, Blackburn M, Rivkees SA. 2003. A1 adenosine receptors mediate hypoxia-induced ventriculomegaly. Proc Natl Acad Sci USA. 100: 11718–11722.

Verma R, Mori S, Shen D, Yarowsky P, Zhang J, Davatzikos C. 2005. Spatiotemporal maturation patterns of murine brain quantified by diffusion tensor MRI and deformation-based morphometry. Proc Natl Acad Sci USA. 102:6978–6983.

Vincze A, Mazlo M, Seress L, Komoly S, Abraham H. 2008. A correlative light and electron microscopic study of postnatal myelination in the murine corpus callosum. Int J Dev Neurosci. 26:575–584.

Volpe JJ. 1990. Brain injury in the premature infant: is it preventable? Pediatr Res. 27:S28–33.

Volpe JJ. 1997. Brain injury in the premature infant. Clin Perinatol. 24:567–587.

Volpe JJ. 2003. Cerebral white matter injury of the premature infant-more common than you think. Pediatrics. 112:176–180.

Waxman SG, Black JA, Kocsis JD, Ritchie JM. 1989. Low density of sodium channels supports action potential conduction in axons of neonatal rat optic nerve. Proc Natl Acad Sci USA. 86:1406–1410.

Westin CF, Maier SE, Mamata H, Nabavi A, Jolesz FA, Kikinis R. 2002. Processing and visualization for diffusion tensor MRI. Med Image Anal. 6:93–108.

Xue R, van Zijl PC, Crain BJ, Solaiyappan M, Mori S. 1999. In vivo three-dimensional reconstruction of rat brain axonal projections by diffusion tensor imaging. Magn Reson Med. 42:1123–1127.

Zhang J, Richards LJ, Yarowsky P, Huang H, van Zijl PC, Mori S. 2003. Three-dimensional anatomical characterization of the developing mouse brain by diffusion tensor microimaging. Neuroimage. 20:1639–1648.

Zhang J, van Zijl PC, Mori S. 2002. Three-dimensional diffusion tensor magnetic resonance microimaging of adult mouse brain and hippocampus. Neuroimage. 15:892–901.

Zhou D, Wang J, Zapala MA, Xue J, Schork NJ, Haddad GG. 2008. Gene expression in mouse brain following chronic hypoxia: role of sarcospan in glial cell death. Physiol Genomics. 32:370–379.